Available online at www.sciencedirect.com
ScienceDirect
International Journal of Solids and Structures 44 (2007) 2523–2539
INTERNATIONAL JOURNAL OF SOLIDS and STRUCTURES
www.elsevier.com/locate/ijsolstr

A coupled FEM/BEM approach and its accuracy for solving crack problems in fracture mechanics

B. Aour [a,*], O. Rahmani [b], M. Nait-Abdelaziz [a]

[a] *Laboratory of Mechanics of Lille, Polytech'Lille USTL, P. Langevin Avenue, 59655 Villeneuve d'Ascq Cedex, France*
[b] *Laboratory of Applied Mechanics, Department of Mechanical Engineering, University of Sciences and Technology of Oran, Algeria*

Received 23 July 2005; received in revised form 2 May 2006
Available online 8 August 2006

Abstract

The finite element (FEM) and the boundary element methods (BEM) are well known powerful numerical techniques for solving a wide range of problems in applied science and engineering. Each method has its own advantages and disadvantages, so that it is desirable to develop a combined finite element/boundary element method approach, which makes use of their advantages and reduces their disadvantages. Several coupling techniques are proposed in the literature, but until now the incompatibility of the basic variables remains a problem to be solved. To overcome this problem, a special super-element using boundary elements based on the usual finite element technique of total potential energy minimization has been developed in this paper. The application of the most commonly used approaches in finite element method namely quarter-point elements and J-integrals techniques were examined using the proposed coupling FEM–BEM. The accuracy and efficiency of the proposed approach have been assessed for the evaluation of stress intensity factors (SIF). It was found that the FEM–BEM coupling technique gives more accurate values of the stress intensity factors with fewer degrees of freedom.

Keywords: Coupling FEM–BEM; Direct boundary element method; Fracture mechanics; Stress intensity factors

1. Introduction

The general technique of FEM–BEM coupling was developed in a classical paper by Zienkiewicz et al. (1977). An extensive literature survey on this topic can be found in Li et al. (1986). The development and analysis of new techniques for coupling FEM–BEM have been the subject of growing interest in recent years. It has been investigated extensively and applied to areas such as fluid and solid mechanics, geomechanics, electromagnetics, acoustics, etc. (Beer, 1986; Wearing and Sheikh, 1988; Grannell, 1988; Coda et al., 1997; Schnack and Turke, 1997). Existing coupling approaches can be classified roughly into three main groups: FEM hosted, BEM hosted, and those not belonging to either of these two categories.

* Corresponding author. Tel.: +33 674619650; fax: +33 328767301.
E-mail address: ben_aour@hotmail.com (B. Aour).

0020-7683/$ - see front matter © 2007 Published by Elsevier Ltd.
doi:10.1016/j.ijsolstr.2006.08.001

Nomenclature

$\{b\}$	body force intensity vector
BE	superscript indicating boundary element subdomain
c_{ij}	a tensor dependent on the location of the field point x_f
e	superscript indicating elemental matrices
F_x, F_y	nodal force components in the x- and y-directions, respectively
$\{F\}$	nodal force vector
FE	superscript indicating finite element subdomain
G_{ij}, H_{ij}	Kelvin's solutions
$[G]$, $[H]$	matrices containing fundamental solution parameters
IB	superscript indicating interface boundary element subdomain
IF	superscript indicating interface finite element subdomain
J	Rice's integral
$[K]$	stiffness matrix
K_I	stress intensity factor for mode I
N	number of boundary elements
$N_i(\xi)$	shape functions
n_i	unit direction normal
r	distance between the field point and the source point
R	distance from the crack-tip
S	integration contour for evaluation of J-integral
$\{t_n\}$	vector containing the nodal tractions
t_x, t_y	traction components in the x- and y-directions, respectively
T	superscript indicating transpose of a matrix
$\{u_n\}$	vector containing the nodal displacements
U	strain energy density
u, v	displacement components in the x- and y-directions, respectively
$u_i(x_f)$, $u_i(x_s)$	displacements at field and source points, respectively
W	work done by external loads
x, y	Cartesian coordinates
x_i^e, u_i^e, t_i^e	vector of coordinates of node i on element e, similarly, u and t describe displacements and tractions
x_f, x_s	field and source points, respectively
α	polar angle
Γ	boundary of the domain Ω
$\{\sigma\}$	stress vector
Ω	two-dimensional domain
δ	prefix indicating a finite increment
δ_{ij}	Kronecker symbol
ν	Poisson's ratio
μ	Lamé constant
ξ	local coordinate
Π	total potential energy of the whole domain
$\{\varepsilon\}$	strain vector

The first type essentially treats the subdomain BEM as a macro-finite element (super-element). The displacement–traction equations governing the boundary element subdomain are transformed into displacement–force equations and assembled with those of the finite element method (Wearing and Sheikh, 1988; Ganguly et al., 2000; Aour, 1997; Aour et al., 2005). Conversely, the BEM approach treats the FE subdomain

as an equivalent BE subregion by converting the stiffness equations of the FEM to BEM-like equations and coupled with those of the BEM while satisfying continuity and equilibrium along the interface (Zienkiewicz et al., 1977; Brebbia and Georgiou, 1979). Approaches not categorized within either of these two groups include direct coupling. These approaches are difficult and inefficient due to the large number of unknowns (Ganguly et al., 2000). One of these approaches is that of boundary coupling (Hsiao, 1988), in which the governing equations of one subdomain are treated as the boundary conditions for the other. In the same principle, an alternative method named as iterative domain decomposition coupling is developed by Chia-Ching et al. (1996) and improved by Elleithy et al. (2001); in which the original problem is solved by continuously adjusting the unbalanced forces or displacements from the subdomains to the artificial interface until continuity and equilibrium are satisfied. The disadvantage of this group of technique is that at each iteration step the boundary problems in BEM and FEM subregions should be solved. As the convergence of the process can be slow, this may lead to long CPU times.

In general, each type of coupling approach has its merits and limitations. In this paper a new method based on the FE approach is developed for coupling the FEM and the BEM. A technique has therefore been developed which modifies the direct BEM using the usual finite element technique of minimization of total potential energy to produce a final system of equations, which are compatible with those of the FEM. The equations for the boundary element region are then used by a standard finite element program as a super-element. The advantage of this approach is that it is easily implemented in a finite element program without major modifications and does not require iterative calculations, which weighs down the convergence solution.

In what follows we shall first introduce the basic formulation of the boundary element method. Then, the procedure for coupling both methods and its implementation in a computer code are discussed in detail. The accuracy and efficiency of the proposed approach have been assessed by the evaluation of stress intensity factors (SIF) using two examples of fracture mechanics.

2. BEM formulation

The main objective of this section is to give an overview of the direct boundary element adaptation to the FEM–BEM coupling for stress analysis. As it is well known there are many engineering topics where boundary element methods (BEM) have been applied, see for instance some recent works (Alvarez-Rubio et al., 2005; Popov and Power, 2001; Brebbia, 1981; Banerjee and Butterfield, 1981). The term BEM (for Boundary Element Method) was first introduced in the 1970s by Brebbia and has been used extensively since then. The method is based on the discretization of the classical Somigliana's identity, which stems from the reciprocity work theorem. This equation is given in terms of the Green's function, which is the full-space harmonic steady-state fundamental solution. For more details see Brebbia (1981) or Banerjee and Butterfield (1981). For a body of domain Ω with a boundary Γ and in the absence of the body forces, the displacement boundary integral equations for elasticity can be written as

$$c_{ij}(x_{\mathrm{f}})u_i(x_{\mathrm{f}}) + \int_{\Gamma} H_{ij}(x_{\mathrm{f}}, x_{\mathrm{s}})u_j(x_{\mathrm{s}})\,\mathrm{d}\Gamma = \int_{\Gamma} G_{ij}(x_{\mathrm{f}}, x_{\mathrm{s}})t_j(x_{\mathrm{s}})\,\mathrm{d}\Gamma \tag{1}$$

where the term c_{ij} is a function of the geometry at the boundary location x_{f}. Providing x_{f} is a smooth boundary point, that is, the outward normal vector to the boundary is continuous at x_{f}, and then it can be shown that $c_{ij} = +1/2\ \delta_{ij}$. The kernels $H_{ij}(x_{\mathrm{f}}, x_{\mathrm{s}})$ and $G_{ij}(x_{\mathrm{f}}, x_{\mathrm{s}})$ are Kelvin's solutions, see Brebbia (1981) or Banerjee and Butterfield (1981). They are known as the fundamental solutions of the elasticity problem and for 2 dimensional plane strain problems are given as

$$G_{ij}(x_{\mathrm{f}}, x_{\mathrm{s}}) = \frac{1}{8\pi\mu(1-\nu)}\left[(1-4\nu)\delta_{ij}\ln\frac{1}{r} + r_{,i}r_{,j}\right] \tag{2}$$

$$H_{ij}(x_{\mathrm{f}}, x_{\mathrm{s}}) = \frac{-1}{4\pi(1-\nu)r}\left\{\frac{\partial r}{\partial n}\left[(1-2\nu)\delta_{ij} + 2r_{,i}r_{,j}\right] + (1-2\nu)(n_i r_{,j} - n_j r_{,i})\right\} \tag{3}$$

where $r = \sqrt{r_i r_i}$, $r_i = y_i - x_i$, $r_{,i} = \partial r/\partial y_i = r_i/r$ and $\partial r/\partial n = r_{,i}n_i$. The physical explanation of $G_{ij}(x_{\mathrm{f}}, x_{\mathrm{s}})$ and $T_{ij}(x_{\mathrm{f}}, x_{\mathrm{s}})$ is that they represent the displacements and tractions in the j direction at the field point x_{f} due to a concentrated unit load in the i direction acting at the loading or source point x_{s} (Fig. 1).

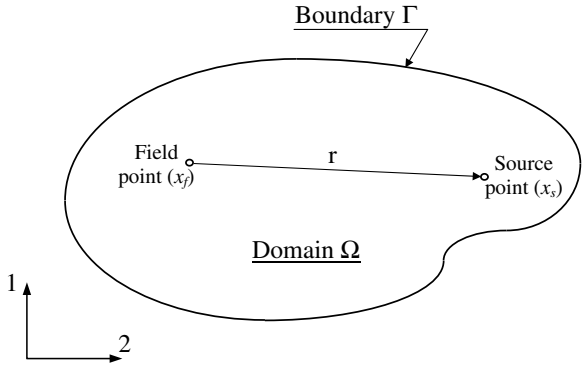

Fig. 1. Source and field point relationship.

The solution of Eq. (1) is achieved by discretizing the boundary Γ of the domain Ω into N boundary elements. The numerical procedure requires the use of interpolation functions, by which the shape of the element and the distribution of displacement and traction components over each boundary element is approximated in terms of their values at the nodes, i.e.

$$x(\xi) = \sum_{i=1}^{3} N_i(\xi) x_i^e \tag{4a}$$

$$u(\xi) = \sum_{i=1}^{3} N_i(\xi) u_i^e \tag{4b}$$

$$t(\xi) = \sum_{i=1}^{3} N_i(\xi) t_i^e \tag{4c}$$

where $N_i(\xi)$ are the shape functions of an isoparametric quadratic boundary element. The discretized form of Eq. (1) for a nodal point P on the boundary can now be written as

$$c^P u^P + \sum_{e=1}^{N} \sum_{i=1}^{3} \left[\int_{\Gamma^e} H_{ij}(x_\mathrm{f}, x_\mathrm{s}) N_i(\xi)\, \mathrm{d}\Gamma \right] u_i^e = \sum_{e=1}^{N} \sum_{i=1}^{3} \left[\int_{\Gamma^e} G_{ij}(x_\mathrm{f}, x_\mathrm{s}) N_i(\xi)\, \mathrm{d}\Gamma \right] t_i^e \tag{5}$$

where the summation is for N elements and i element nodes.

By taking the field point successively to all the nodal points on the boundary and by assembling the equations into a block matrix, we obtain

$$[H]\{u_n\} = [G]\{t_n\} \tag{6}$$

where $[H]$ and $[G]$ denote the influence coefficient matrices which are obtained by integration over the boundary elements using the fundamental solutions, $\{u_n\}$ and $\{t_n\}$ are the vectors containing the nodal displacements and tractions, respectively.

Noting that, to follow the matrix algebra it is useful to consider the matrix sizes. In the presence of the corners the matrix $[H]$ related to displacements remains always square of order $(2M \times 2M)$ if M is the total number of the geometrical nodes. This property is due to the unicity of displacements at the corners. On the other hand the matrix $[G]$ becomes a rectangular matrix of order $2M \times (2M + 2m)$ if m is the number of corners appearing on the geometry.

3. Coupling procedure

The finite element and boundary element methods have dissimilar final sets of equations. The finite element method results in a force–displacement equations system. However, the boundary element method produces a system of simultaneous equations relating the nodal displacements and nodal tractions. This makes it possible

to create a link between the two methods (Oysu and Fenner, 2006). It is more appropriate to use the FE approach for the coupling since the finite element is well established in the industrial environment. The equations of the subdomain previously discretized using boundary elements, can be easily solved by finite elements codes. In what follows, we consider a subdomain Ω^{FE} with boundary Γ^{FE} discretized by finite elements and a subdomain $\Omega^{BE}$of boundary Γ^{BE} discretized by boundary elements (Fig. 2).

The final set of finite element and boundary element equations for the two subdomains, which are connected at a common interface, can be respectively written in matrix form as

$$[K]^{FE}\{u\}^{FE} = \{F\}^{FE} \tag{7}$$

$$[H]^{BE}\{u\}^{BE} = [G]^{BE}\{t\}^{BE} \tag{8}$$

where $[K]^{FE}$ is the stiffness matrix for the finite element subdomain, $\{u\}^{FE}$ and $\{F\}^{FE}$ are the nodal displacement and force vectors respectively, $[H]^{BE}$ and $[G]^{BE}$ are the influence coefficient matrices, and $\{u\}^{BE}$ and $\{t\}^{BE}$ are the displacement and traction vectors of the boundary element subdomain.

It is understood that the governing equations in the FE subdomain involve nodal displacements and forces; whereas, the primary unknowns in the BE subdomain are displacements and tractions. To facilitate the FEM–BEM coupling, we need to determine the nodal forces and the equivalent stiffness matrix of the boundary element subdomain.

3.1. Determination of the nodal forces

The virtual work principle ensures that along the interface, the work done by the nodal point force F^e and the interface traction t^e on an arbitrary virtual displacement δu^e are equal. So, for the boundary element "e" (Fig. 3), this leads to

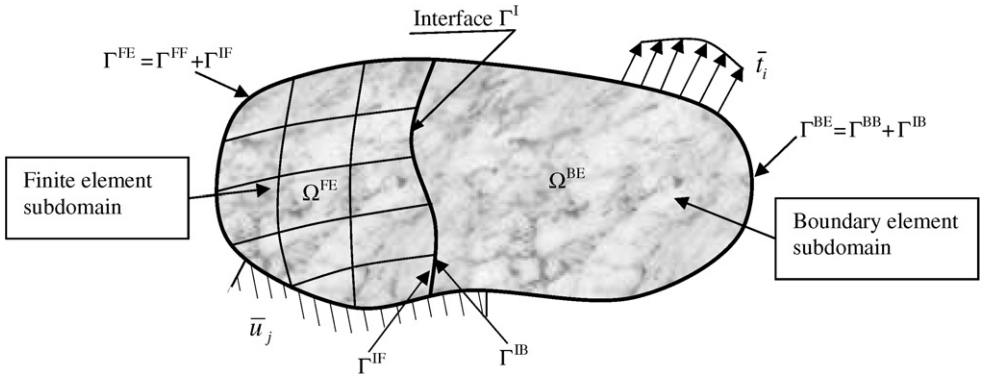

Fig. 2. Discretization of two-dimensional body with FEM–BEM.

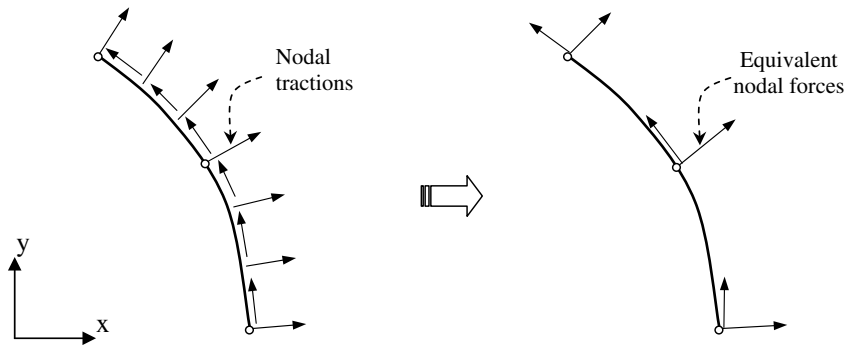

Fig. 3. Loaded boundary element.

$$\delta W^e = (\delta u^e)^{\mathrm{T}} F^e \tag{9}$$

The work done by the applied tractions during virtual displacements δu in the x-direction and δv in the y-direction can be expressed as follows:

$$\delta W^e = \int_\Gamma (t_x \delta u + t_y \delta v)\, \mathrm{d}\Gamma \tag{10}$$

Writing t_x, t_y, δu and δv in terms of their nodal values, i.e.

$$\delta u(\xi) = \sum_{i=1}^{3} N_i(\xi) \cdot \delta u_i^e, \quad \delta v(\xi) = \sum_{i=1}^{3} N_i(\xi) \cdot \delta v_i^e \tag{11}$$

$$t_x(\xi) = \sum_{j=1}^{3} N_j(\xi) \cdot (t_x^e)_j, \quad t_y(\xi) = \sum_{j=1}^{3} N_j(\xi) \cdot (t_y^e)_j \tag{12}$$

then Eq. (10) can be rewritten as follows:

$$\delta W = \sum_{i=1}^{3} \left[\delta u_i \sum_{j=1}^{3} \left\{ (t_x)_i \int_\Gamma N_i(\xi) N_j(\xi)\, \mathrm{d}\Gamma \right\} + \sum_{j=1}^{3} \left\{ (t_y)_i \int_\Gamma N_i(\xi) N_j(\xi)\, \mathrm{d}\Gamma \right\} \delta v_i \right] \tag{13}$$

The corresponding work done by the equivalent nodal force vector is

$$\delta W = \sum_{i=1}^{3} [(F_x)_i \delta u_i + (F_y)_i \delta v_i] \tag{14}$$

Comparing Eq. (10) with Eq. (13), it can be deduced that

$$(F_x)_i = \sum_{j=1}^{3} (t_x)_i \int_\Gamma N_i(\xi) N_j(\xi)\, \mathrm{d}\Gamma \tag{15}$$

$$(F_y)_i = \sum_{j=1}^{3} (t_y)_i \int_\Gamma N_i(\xi) N_j(\xi)\, \mathrm{d}\Gamma \tag{16}$$

The integration is performed using Gaussian quadrature. Therefore, an element nodal force vector F^e may be expressed in terms of an element nodal traction vector t^e as follows:

$$F^e = M^e t^e \tag{17}$$

where M^e is the converting matrix, which depends on the interpolation functions as follows:

$$M^e = \begin{bmatrix}
\int_{-1}^{+1} N_1 N_1 J\, \mathrm{d}\xi & 0 & \int_{-1}^{+1} N_1 N_2 J\, \mathrm{d}\xi & 0 & \int_{-1}^{+1} N_1 N_3 J\, \mathrm{d}\xi & 0 \\
0 & \int_{-1}^{+1} N_1 N_1 J\, \mathrm{d}\xi & 0 & \int_{-1}^{+1} N_1 N_2 J\, \mathrm{d}\xi & 0 & \int_{-1}^{+1} N_1 N_3 J\, \mathrm{d}\xi \\
\int_{-1}^{+1} N_2 N_1 J\, \mathrm{d}\xi & 0 & \int_{-1}^{+1} N_2 N_2 J\, \mathrm{d}\xi & 0 & \int_{-1}^{+1} N_2 N_3 J\, \mathrm{d}\xi & 0 \\
0 & \int_{-1}^{+1} N_2 N_1 J\, \mathrm{d}\xi & 0 & \int_{-1}^{+1} N_2 N_2 J\, \mathrm{d}\xi & 0 & \int_{-1}^{+1} N_2 N_3 J\, \mathrm{d}\xi \\
\int_{-1}^{+1} N_3 N_1 J\, \mathrm{d}\xi & 0 & \int_{-1}^{+1} N_3 N_2 J\, \mathrm{d}\xi & 0 & \int_{-1}^{+1} N_3 N_3 J\, \mathrm{d}\xi & 0 \\
0 & \int_{-1}^{+1} N_3 N_1 J\, \mathrm{d}\xi & 0 & \int_{-1}^{+1} N_3 N_2 J\, \mathrm{d}\xi & 0 & \int_{-1}^{+1} N_3 N_3 J\, \mathrm{d}\xi
\end{bmatrix} \tag{17a}$$

$$F^{e^{\mathrm{T}}} = \{ (F_x)_1 \quad (F_y)_1 \quad (F_x)_2 \quad (F_y)_2 \quad (F_x)_3 \quad (F_y)_3 \} \tag{17b}$$

$$t^{e^{\mathrm{T}}} = \{ (t_x)_1 \quad (t_y)_1 \quad (t_x)_2 \quad (t_y)_2 \quad (t_x)_3 \quad (t_y)_3 \} \tag{17c}$$

The consequence of Eq. (17) is that the boundary element region can be treated as a "super-element" and its stiffness matrix and load vector can be assembled with the finite element matrices in the usual way.

3.2. Determination of the global stiffness matrix

3.2.1. Principle of total potential energy minimization

To determine the equivalent stiffness matrix of the super-element, we use the principle of total potential energy minimization and the direct boundary element method presented in the previous section. The total potential energy of the whole domain Ω with a contour Γ (Fig. 2) is given as

$$\Pi = \frac{1}{2}\int_{\Omega}[\sigma]^{\mathrm{T}}\{\varepsilon\}\,\mathrm{d}\Omega - \int_{\Omega}\{u\}^{\mathrm{T}}\{b\}\,\mathrm{d}\Omega - \int_{\Gamma}\{u\}^{\mathrm{T}}\{p\}\,\mathrm{d}\Gamma \tag{18}$$

where the first term is a volume integral of the strain energy density and the last two integrals are the external work terms. $[\sigma]$ and $\{\varepsilon\}$ are stress and strain vectors respectively, $\{b\}$ is the body forces vector and $\{p\}$ is the external boundary loads vector. Integrations are taken over the domain Ω of the structure and the loaded contour Γ.

For the two subdomains the above expression can be rewritten as follows:

$$\begin{aligned}\Pi = {} & \frac{1}{2}\int_{\Omega^{\mathrm{FE}}}[\sigma]^{\mathrm{T}}\{\varepsilon\}\,\mathrm{d}\Omega - \int_{\Omega^{\mathrm{FE}}}\{u\}^{\mathrm{T}}\{b\}\,\mathrm{d}\Omega - \int_{\Gamma^{\mathrm{FF}}}\{u\}^{\mathrm{T}}\{p\}\,\mathrm{d}\Gamma + \frac{1}{2}\int_{\Omega^{\mathrm{BE}}}[\sigma]^{\mathrm{T}}\{\varepsilon\}\,\mathrm{d}\Omega \\ & - \int_{\Omega^{\mathrm{BE}}}\{u\}^{\mathrm{T}}\{b\}\,\mathrm{d}\Omega - \int_{\Gamma^{\mathrm{BB}}}\{u\}^{\mathrm{T}}\{p\}\,\mathrm{d}\Gamma\end{aligned} \tag{19}$$

where Ω^{FE}, Ω^{BE} represent finite element, boundary element subdomains and Γ^{FF}, Γ^{BB} denote the contours of finite element, boundary element subdomains without interface, such as $\Omega = \Omega^{\mathrm{FE}} + \Omega^{\mathrm{BE}}$ and $\Gamma = \Gamma^{\mathrm{FF}} + \Gamma^{\mathrm{BB}}$.

At the interface, the compatibility and equilibrium conditions should be satisfied, i.e.

$$u^{\mathrm{IF}} = u^{\mathrm{IB}} \quad \text{on } \Gamma^{I} \tag{20}$$

$$t^{\mathrm{IF}} + t^{\mathrm{IB}} = 0 \quad \text{on } \Gamma^{I} \tag{21}$$

From these two conditions, one can write

$$-\int_{\Gamma^{\mathrm{IF}}}\{u^{\mathrm{IF}}\}^{\mathrm{T}}\{t^{\mathrm{IF}}\}\,\mathrm{d}\Gamma - \int_{\Gamma^{\mathrm{IB}}}\{u^{\mathrm{IB}}\}^{\mathrm{T}}\{t^{\mathrm{IB}}\}\,\mathrm{d}\Gamma = 0 \tag{22}$$

Combining this with Eq. (19) allows the potential energy of the whole region to be split into the sum of energies for the two subdomains

$$\Pi = \Pi^{\mathrm{FE}} + \Pi^{\mathrm{BE}} \tag{23}$$

where Π^{FE} and Π^{BE} are respectively the total potential energy for the FEM and BEM subdomains.

For the finite element subdomain, we obtain immediately the expression (7) by minimizing Π^{FE}. But for the boundary element subdomain, to determine the equivalent stiffness matrix, some mathematical transformations are required.

First, by applying the divergence theorem and using the stresses equilibrium equations, in the absence of the body forces, we can write

$$\frac{1}{2}\int_{\Omega^{\mathrm{BE}}}[\sigma]^{\mathrm{T}}\{\varepsilon\}\,\mathrm{d}\Omega = \frac{1}{2}\int_{\Gamma^{\mathrm{BE}}}\{u\}^{\mathrm{T}}\{t\}\,\mathrm{d}\Gamma \tag{24}$$

where $\{t\}$ are tractions due to displacements.

Substituting Eq. (24) in the expression of Π^{BE}, we obtain

$$\Pi^{\mathrm{BE}} = \frac{1}{2}\int_{\Gamma^{\mathrm{BE}}}\{u\}^{\mathrm{T}}\{t\}\,\mathrm{d}\Gamma - \int_{\Omega^{\mathrm{BE}}}\{u\}^{\mathrm{T}}\{b\}\,\mathrm{d}\Omega - \int_{\Gamma^{\mathrm{BE}}}\{u\}^{\mathrm{T}}\{p\}\,\mathrm{d}\Gamma \tag{25}$$

By expressing the displacements and tractions vectors in terms of their nodal values, Eq. (25) in the absence of the body forces becomes

$$\Pi^{\mathrm{BE}} = \frac{1}{2}\{u_n\}^{\mathrm{T}}\left(\int_{\Gamma^{\mathrm{BE}}}[N]^{\mathrm{T}}[N]\,\mathrm{d}\Gamma\right)\{t_n\} - \{u_n\}^{\mathrm{T}}\left(\int_{\Gamma^{\mathrm{BE}}}[N]^{\mathrm{T}}\{p\}\,\mathrm{d}\Gamma\right) \tag{26}$$

3.2.2. Solution strategy on interface and corners

Considering now the direct boundary element method presented in Section 2; in the case of smooth contours (Fig. 4(a)), the matrix G always remains a square and invertible matrix. So the calculation of the equivalent stiffness matrix for the BEM subregion can be directly achieved. In contrast, when the domain exhibits geometric corners (Fig. 4(b)), an additional difficulty appears because the outward normal at the node located at the corner is undefined. Corner problems within the scope of BEM have been approached in literature. Brebbia (1981) proposed the use of non-conforming elements, which avoids placing a boundary node exactly at the corner. This node is replaced by two non-coincident nodes near the corner allowing to remove the discontinuity. Consequently, this method fails to determine the stresses at the corner. Chan and Chandra (1991) developed a method for a BEM solution of steady-state heat conduction that places only one node at the corner. More recently, Guven and Madenci (2003) then extended this method to thermoelastic stress analysis for a specific class of boundary conditions.

The approach proposed in this work is based on the same double node concept in which two boundary nodes are placed at the corner with exactly the same coordinates. After this, we preserve only the node compatible with the loading and deformations conditions of this material point. At this stage special care has to be taken for the corner nodes of interface and boundary element subregion:

Case 1: Corner nodes at interface

Consider FEM and BEM nodes on the interface corner elements as shown in Fig. 5. In this case we consider only the contributions of the elements interfacing the FEM region. For instance, for the boundary elements (a) and (b), we consider only the contributions of element (b), i.e. $t_i^c \equiv t_i^b$ and $t_i^a = 0$, where t_i^c denote the nodal value of traction preserved at the corner node, t_i^a and t_i^b are the nodal values of tractions close to the corner of element (a) and (b), respectively.

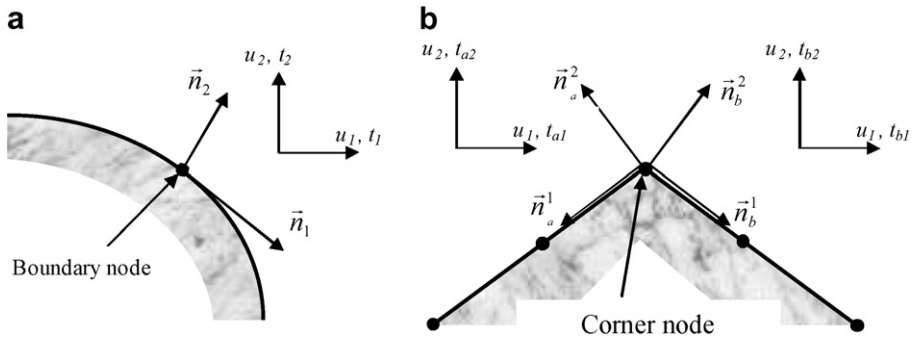

Fig. 4. Boundary point positions: (a) smooth contour; (b) sharp contour.

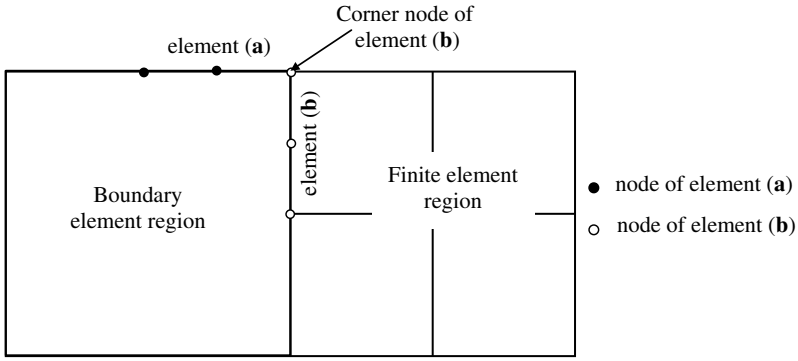

Fig. 5. Selection of the corner nodes on interface.

If the displacement boundary conditions are described on the element (a), this time element (a) will contribute to corner node for traction calculations outside the interface.

Case 2: Corner nodes of BEM region without interface

If the surface tractions are prescribed as shown in Fig. 6(a), we preserve only the contributions of the element (b). If the displacement boundary conditions are fixed on the element (a) (Fig. 6(b)), then the contributions of element (a) will be taken into consideration. In the case when the tractions are specified before and after the corner (Fig. 6(c)), we preserve either and the tractions contribution is the average of both. Finally, the case, when only the displacements are specified at the corner (Fig. 6(d)), is not treated in this paper and an alternative approach is given by Schnack and Turke (1997).

3.2.3. Equivalent stiffness matrix for the super-element and assembly of matrices

By using the previous approach, only common corner node is used and the matrix $[G]$ becomes a square and invertible matrix. Consequently, we can write the system of boundary element Eq. (7), as follows:

$$[G]^{-1}[H]\{u_n\} = \{t_n\} \tag{27}$$

where the inverse of the matrix $[G]$ is calculated by Gaussian elimination (Adey and Brebbia, 1983), which has been proved and commonly used by several authors in continuum mechanics. Noting that, an investigation of other methods for which an inverse is safe, could prove extremely beneficial.

Substituting the expression (27) in (26) when the external loads $\{p\}$ correspond to a surface traction $\{t\}$, we obtain

$$\Pi^{\mathrm{BE}} = \frac{1}{2}\{u_n\}^{\mathrm{BE^T}}[M][G]^{-1}[H]\{u_n\}^{\mathrm{BE}} - \{u_n\}^{\mathrm{BE^T}}\left(\int_{\Gamma^{\mathrm{BE}}}[N]^{\mathrm{T}}[N]\{t_n\}\,\mathrm{d}\Gamma\right) \tag{28}$$

or more compactly

$$\Pi^{\mathrm{BE}} = \frac{1}{2}\{u_n\}^{\mathrm{BE^T}}[K]^{\mathrm{BE}}\{u_n\}^{\mathrm{BE}} - \{u_n\}^{\mathrm{BE^T}}\{F\}^{\mathrm{BE}} \tag{29}$$

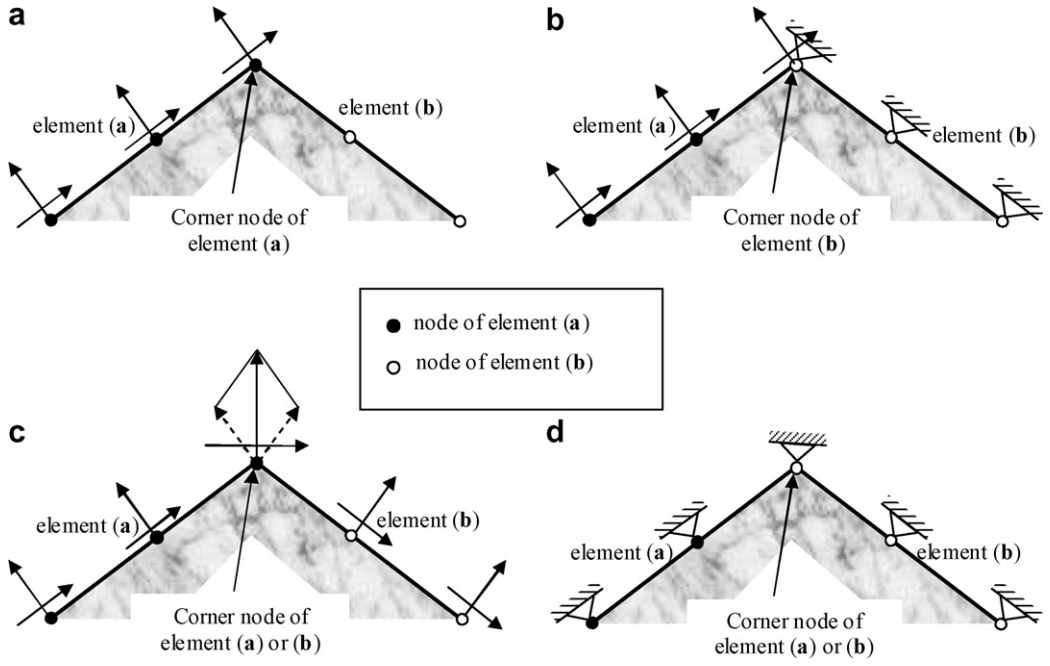

Fig. 6. Selection of the corner nodes out interface.

with

$$[K]^{\mathrm{BE}} = [M][G]^{-1}[H] \quad \text{and} \quad \{F\}^{\mathrm{BE}} = \int_{\Gamma^{\mathrm{BE}}} [N]^{\mathrm{T}}[N]\{t_n\}\,\mathrm{d}\Gamma \tag{30}$$

Minimizing the functional Π^{BE} with respect to nodal displacements, gives

$$[K]^{\mathrm{BE}}\{u_n\}^{\mathrm{BE}} = \{F\}^{\mathrm{BE}} \tag{31}$$

where $[K]^{\mathrm{BE}}$ is the equivalent rigidity matrix of the super-element BE and $\{F\}^{\mathrm{BE}}$ its equivalent nodal forces. $[K]^{\mathrm{BE}}$ is generally asymmetric due to the approximation involved in the discretization process and the choice of the assumed solution. Although this matrix is sometimes symmetrized by simply taking an average of the off-diagonal terms (i.e. assuming it can be written as $\frac{1}{2}([K]^{\mathrm{BE}} + [K]^{\mathrm{BE^T}})$) this is not recommended as it produces inaccurate results in many practical applications (Brebbia and Dominguez, 1992; Hunter, 2001). Obtaining symmetric boundary element stiffness matrices may involve double integration of the type used in Galerkin's boundary element formulation, which are beyond the scope of this paper.

The matrices of Eq. (31) can now be assembled with matrices corresponding to FE subregion to form the global stiffness matrix. Considering the two subregions described in Fig. 1, Eqs. (7) and (31) can be further partitioned into those associated to the interface, and those disassociated from the interface as

$$\begin{bmatrix} K^{\mathrm{FF}} & K^{\mathrm{FI}} \\ K^{\mathrm{IF}} & K^{\mathrm{II}} \end{bmatrix} \begin{Bmatrix} u^{\mathrm{F}} \\ u^{\mathrm{I}} \end{Bmatrix} = \begin{Bmatrix} F^{\mathrm{F}} \\ F^{\mathrm{IF}} \end{Bmatrix} \tag{32}$$

$$\begin{bmatrix} K^{\mathrm{BB}} & K^{\mathrm{BI}} \\ K^{\mathrm{IB}} & K^{\mathrm{II}} \end{bmatrix} \begin{Bmatrix} u^{\mathrm{B}} \\ u^{\mathrm{I}} \end{Bmatrix} = \begin{Bmatrix} F^{\mathrm{B}} \\ F^{\mathrm{IB}} \end{Bmatrix} \tag{33}$$

where superscripts F, B and I represent finite element, boundary element and interface, respectively.

Consequently, the coupled equation system of the whole domain is obtained by using the standard assembly of the two partial systems as follows:

$$\begin{bmatrix} K^{\mathrm{BB}} & K^{\mathrm{BI}} & 0 \\ K^{\mathrm{IB}} & K^{\mathrm{I}} & K^{\mathrm{FI}} \\ 0 & K^{\mathrm{IF}} & K^{\mathrm{FF}} \end{bmatrix} \begin{Bmatrix} u^{\mathrm{B}} \\ u^{\mathrm{I}} \\ u^{\mathrm{F}} \end{Bmatrix} = \begin{Bmatrix} F^{\mathrm{B}} \\ F^{\mathrm{IB}} + F^{\mathrm{IF}} \\ F^{\mathrm{F}} \end{Bmatrix} \tag{34}$$

By solving the system (34), we can obtain all the unknown displacements and nodal forces of the problem discretized by FEM–BEM.

4. Application to fracture mechanics

The existence of crack-like flaws cannot be excluded in pressured vessels and pipes. Therefore, the interdisciplinary related to pressurized components is of considerable importance in many branches of industry, such as energy, petrochemicals, process plants, transport and space communications. In order to provide a safe service condition, it is important to perform a fracture mechanics assessment.

Among the fracture Modes (I, II and III), Mode-I, also called the opening mode, and its associated parameter K_{I}, is the most important. K_{I} characterizes the stress field in the neighbourhood of a crack-tip when the crack is under tension. Knowledge of K_{I} is essential to establish if an existing crack, under given loading conditions, is stable or not (Bezerra et al., 2001). For simple crack configurations, analytical expressions for K_{I} are available in the literature and in some handbooks. However, for cracks with more complex geometric configuration no handbook method exists for the determination of the stress intensity factor. For complex geometries, the stress intensity factor (SIF) may be obtained by experiments; however, such procedure is expensive when compared to numerical approaches. The use of numerical methods for the determination of K_{I} seems to be an economic tool.

Over the past decade or so a great deal of work has been carried out to develop special techniques for determining accurate values of the stress intensity factor using the finite element method, such as the quarter-point elements (Barsoum, 1976), J-integral (Rice, 1974), strain energy release rate (Griffiths, 1921), virtual crack

extension (Hellen, 1975). Among other numerical methods, the use of coupled FEM–BEM for the computation of K_I appears advantageous since most of the domain is modelled by boundary elements and only a very limited zone in the vicinity of the crack is discretized by finite elements. The finite elements are used near the crack because (a) the fracture parameters can be calculated very easily and accurately by FEM even when nonlinear mechanical behaviour is considered and (b) the BE formulation is well established for linear behaviour and allows a reduction of the system equations size.

4.1. Evaluation techniques of stress intensity factors

In this paper we focus on the application of most commonly used approaches in finite element method, namely quarter-point elements and J-integrals. Crack-tip singularity modelling can be based on special crack-tip elements, which directly model the $1/\sqrt{R}$ tip singularity, where R is the distance from the crack-tip. Following Barsoum (1976), this singularity is most conveniently introduced into a quadratic isoparametric element by shifting the mid-side node to quarter-point position in the direction of the crack-tip. The stress intensity factor is calculated by equating the displacement field on the crack face approximated by the quarter-point element with the first term of near-tip displacement field to give (Owen and Fawkes, 1983)

$$K_I \begin{Bmatrix} (2\kappa-1)\cos\frac{\alpha}{2} - \cos\frac{3\alpha}{2} \\ (2\kappa+1)\sin\frac{\alpha}{2} - \sin\frac{3\alpha}{2} \end{Bmatrix} = 4\mu\sqrt{\frac{2\pi}{R}} \begin{Bmatrix} u \\ v \end{Bmatrix} \tag{35}$$

in which, $\kappa = (3-v)/(1+v)$ for plane stress, $\kappa = 3-4v$ for plane strain, μ is the shear modulus, α is the polar angle, R is the distance from the crack-tip, u and v are the components of displacements.

The stress intensity factor is also related to path-independent integrals, known as J-integrals. For a contour, which encloses the crack-tip and has initial and end points on opposite surfaces of the crack, the Rice's J-integral is defined as (Rice, 1974):

$$J = \int_{\Gamma} \left(U\,\mathrm{d}y - t_i \frac{\partial u_i}{\partial xi}\,\mathrm{d}S \right) \tag{36}$$

where U denotes the strain energy density, u_i represents the displacement vector and t_i represents the traction vector along the elementary arc $\mathrm{d}S$ of the integration contour S. The J-integral is directly related to the stress intensity factor by the relation (Owen and Fawkes, 1983):

$$K_I = \left(\frac{8\mu J}{1+\kappa} \right)^{1/2} \tag{37}$$

4.2. Numerical examples

Before carrying out the implementation and the checking of the coupling technique, we started by implementing and checking the super-element method (SBEM). Consequently, the technique of the super-element has been programmed and tested with several examples before being coupled with the FEM (Aour et al., 2005). To show the efficiency of the proposed method, two techniques allowing the determination of the SIF are implemented in the coupling FEM–BEM program: the displacement extrapolation technique (DET) and the J-integral Technique (JIT). Two different configurations are treated: the first corresponding to a panel with a central crack under uniform traction (Fig. 7(a)) and the second is the same plate but containing two symmetrical cracks emanating from a central circular hole subjected to a uniform traction too. The geometries of the plates and the cracks, the modulus of elasticity and the Poisson's ratio are given in Fig. 7. Due to symmetry conditions, only a quarter of the rectangular plate was discretized with a combined finite elements-boundary elements.

4.2.1. Panel with central crack

In order to test the convergence of the coupling technique for the evaluation of stress intensity factors, three meshes were used as shown in Fig. 8. The first mesh (A) is composed of 12FE coupled with a super-element of

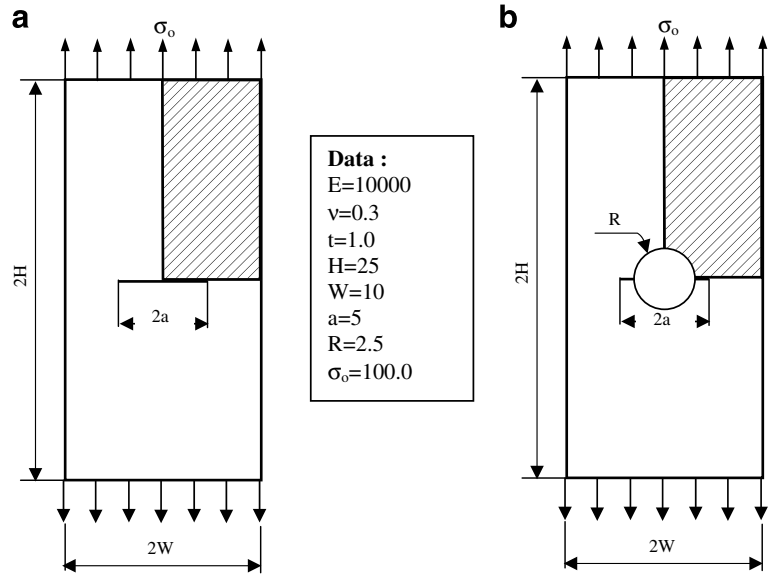

Fig. 7. Crack problems analysed: (a) centre cracked plate, (b) cracks emanating from a circular hole.

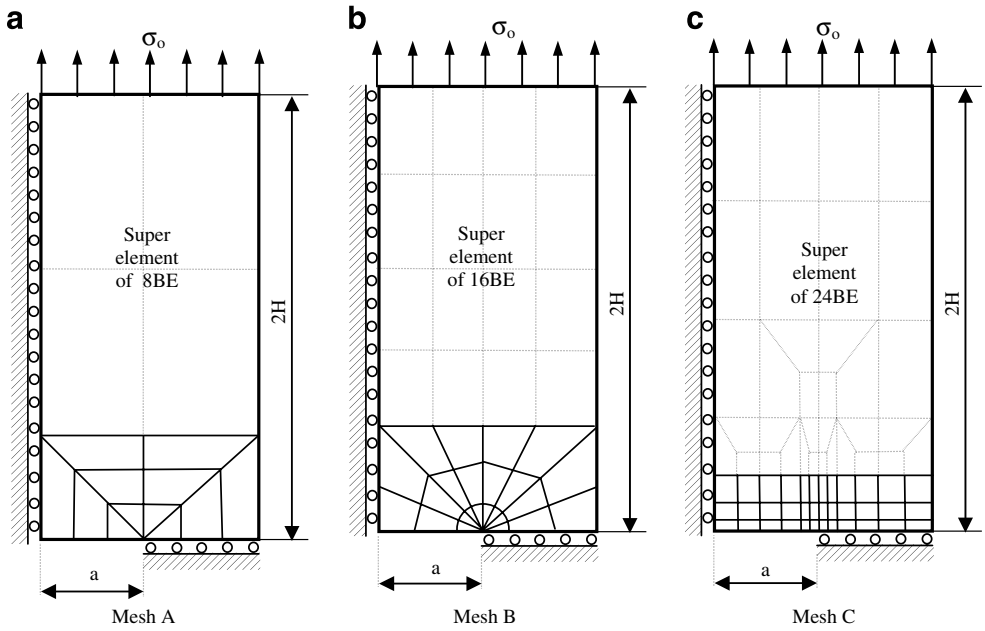

Fig. 8. Various meshes of the central cracked panel.

8BE, the second mesh (B) consists of 24FE combined with a super-element of 16BE and the third mesh (C) is composed of 36FE coupled with a super-element of 24BE. The finite element analysis was carried out on these three meshes with 16, 40 and 70 quadratic elements respectively, as shown in Fig. 8 (fine lines), in such away, we can make a comparison in the same mesh design. To estimate the performance of the proposed method, a comparison of the stress distribution ahead of the crack-tip in the crack line direction between the FEM–BEM technique and the closed-form solutions (Fleming et al., 1997) is depicted in Fig. 9. It can be seen that the numerical results are in a good agreement with the analytical solutions.

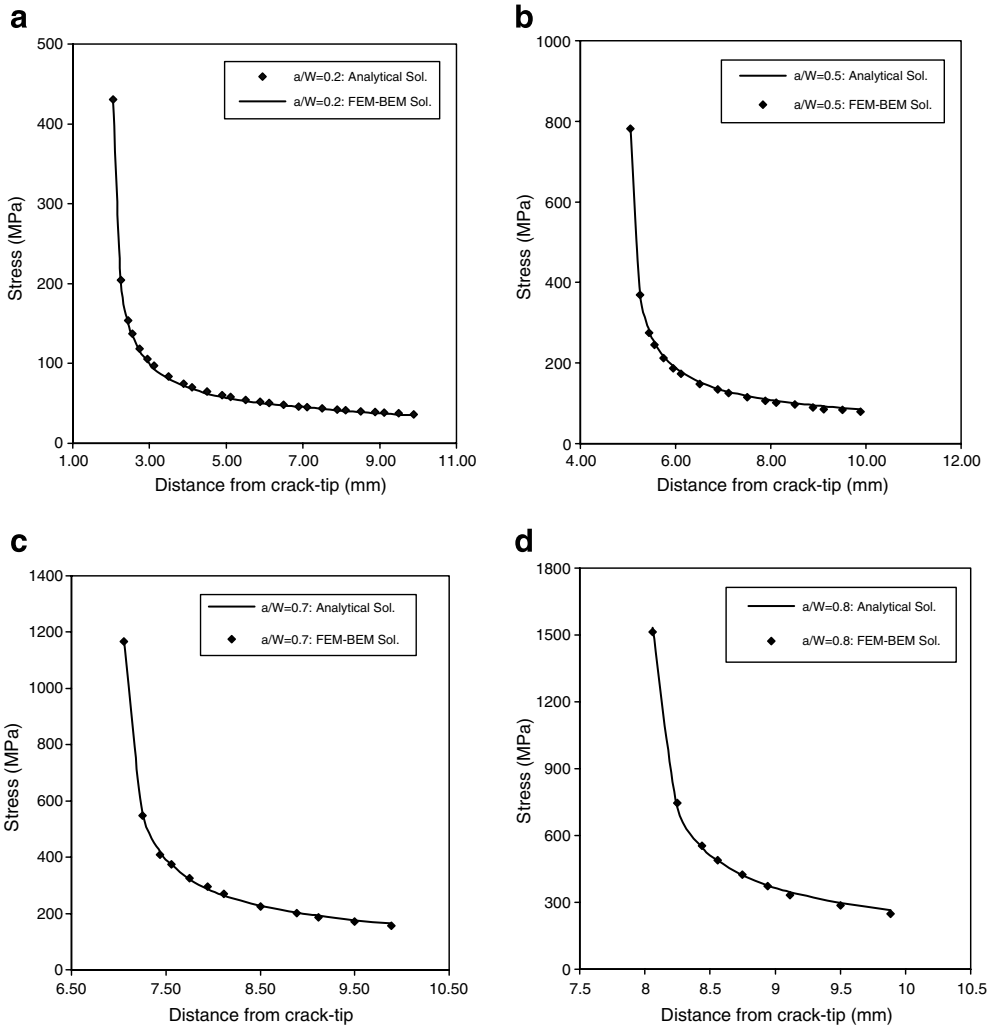

Fig. 9. Opening stresses distributions near the crack-tip ($\theta = 0$ and $R > 0$).

Table 1
K_I values in the case of a central cracked panel ($a/W = 0.5$)

K_I evaluation	Mesh A	Mesh B	Mesh C
FEM–BEM (DET)	463.69	463.88	462.71
FEM (DET)	464.04	463.22	462.01
FEM–BEM (JIT)	462.99	464.12	465.11
FEM (JIT)	461.52	463.69	464.87
Analytical solution		469.14	

The results obtained by using the two techniques DET and JIT are presented in Table 1, and the errors obtained in the calculation of the SIF are plotted in Fig. 10. It can be seen that the best result was achieved with the J-integral technique (JIT). The displacement extrapolation technique with quarter-point elements results appears relatively instable especially for FEM compared to the coupled FEM–BEM. Then, considering the meshing (C) the stress intensity factor K_I corresponding to different relative crack lengths a/W has been computed via the J-integral, using both FEM and FEM–BEM methods.

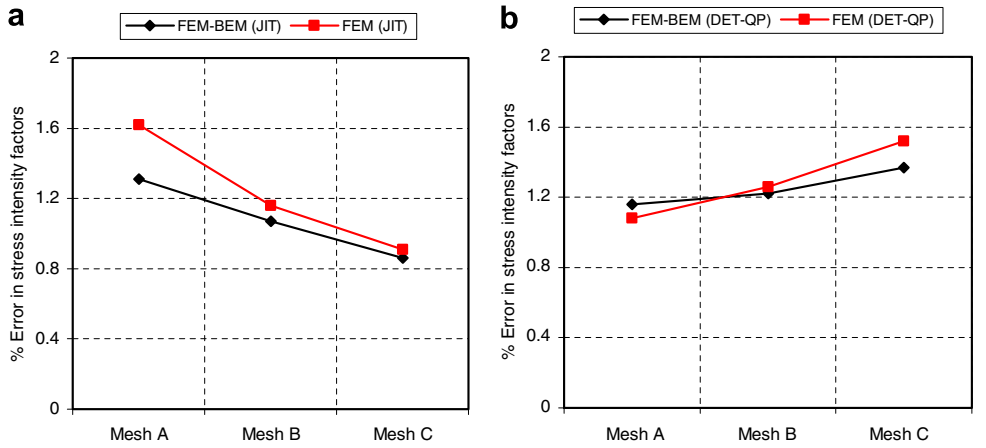

Fig. 10. Error estimation in SIF calculations with (a) J-integral technique (JIT), and (b) displacement extrapolation technique (DET-QP) for $a/W = 0.5$.

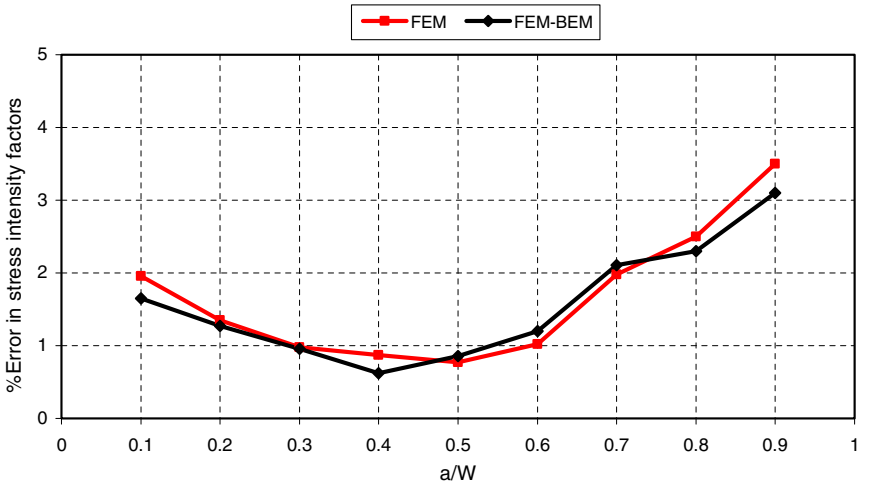

Fig. 11. Error evolution on SIF as function of crack length a/W.

As shown in Fig. 11, the results highlight a very good agreement between FEM and the coupled FEM–BEM for all values of a/W. It can also be seen that both methods are in reasonable agreement with the analytical solution given by Tada et al. (1973).

4.2.2. Cracks emanating from a circular hole

To examine again the DET and JIT techniques for the evaluation of K_I using FEM–BEM approach, three meshes were used, to test the convergence. The first mesh (A) is composed of 11FE coupled with a super-element of 8BE, the second mesh (B) is composed of 25FE combined with a super-element of 16BE and the third mesh (C) is composed of 29FE coupled with a super-element of 22BE. The finite element analysis was carried out on these three meshes with 15, 41 and 58 quadratic elements respectively, as shown in Fig. 12.

The results obtained for this example are presented in Tables 2 and 3 and plotted in Fig. 13. Once again, the tables present the values obtained for the stress intensity factors while the figures illustrate the error obtained in the calculation of K_I using the both FEM and coupled FEM–BEM methods.

It can be seen that, the results of the displacement extrapolation technique with quarter-point elements (Fig. 13(b)), is the least accurate solution among all the configurations tested. The accuracy seems better when

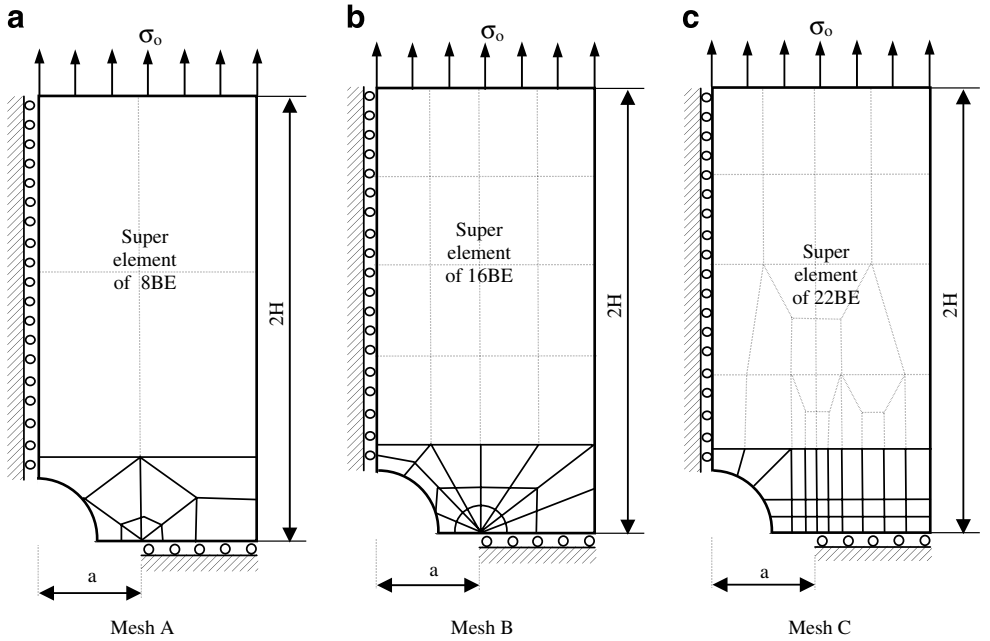

Fig. 12. Various meshes of the panel with cracks emanating from circular hole.

Table 2
K_I values in the case of cracks emanating from a circular hole ($a/W = 0.5$)

K_I evaluation	Mesh A	Mesh B	Mesh C
FEM–BEM (DET)	502.630	496.110	494.735
FEM (DET)	503.344	493.512	489.845
FEM–BEM (JIT)	495.346	502.580	504.210
FEM (JIT)	491.526	501.663	503.547
Woo et al. (1989)		509.406	

Table 3
Stress intensity factors for different a/W

	a/W						
	0.3	0.4	0.5	0.6	0.7	0.8	0.9
FEM–BEM	332.213	426.971	504.210	602.987	730.522	934.863	1357.372
Error	−0.42	0.91	1.02	0.51	1.03	1.43	−2.19
FEM	332.673	427.256	503.547	601.966	730.963	934.185	1365.867
Error	−0.56	0.85	1.15	0.68	0.97	1.51	−2.83
Woo et al. (1989)	330.821	430.919	509.406	606.088	738.123	948.508	1328.277

considering the FEM–BEM technique. The lack of accuracy exhibited by the DET is due to the fact that the quarter-point element solution is dependent on the size of the quarter-point element (Portela and Aliabadi, 1989). The reasons for this size dependence are related to the contradictory requirement of a simultaneous representation of the singular and finite stress terms in a given problem, as it was explained by Harrop (1982). The J-integral approach performance is better than quarter-point element as shown in Fig. 13(a). Table 3 shows a comparison between the solutions obtained from the coupling FEM–BEM and FEM and the results presented by Woo et al. (1989). It can be seen that for all the crack lengths the coupling method results are in good agreement with the FEM and the reference solutions.

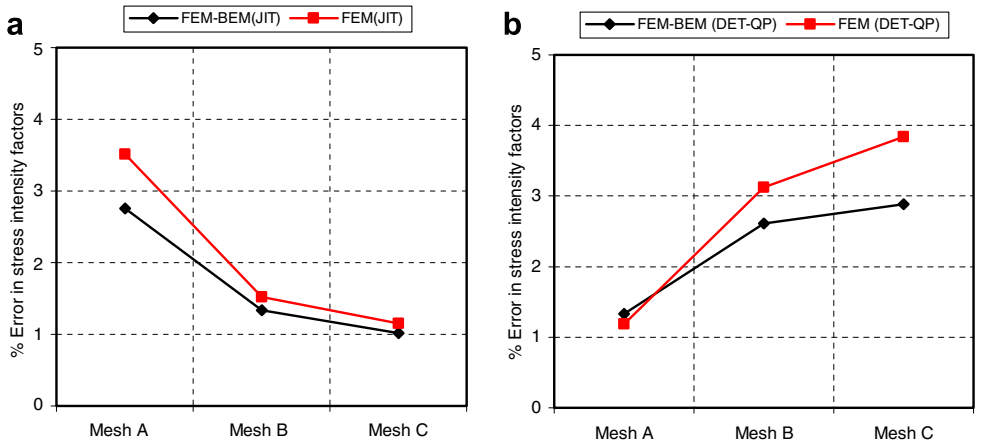

Fig. 13. Error estimation in SIF calculations with (a) J-integral technique (JIT), and (b) displacement extrapolation technique (DET-QP) for $a/W = 0.5$.

5. Conclusions

FEM–BEM coupling was the subject of many investigations and several approaches were proposed in the literature. The originality of this work stems from the development of a new method of boundary elements easy to handle and allowing a fast and effective coupling with the finite element method. This new method of super-element boundary elements is based upon the principle of total potential energy minimization and on the direct boundary element method to determine the equivalent stiffness matrix and the contributions of the nodal forces.

The major advantage of this procedure is that all finite element programs can adapt very easily with the model of super-element BEM. This is due to the optimal properties offered by this model, such as: flexibility of discretizations FEM and BEM, the use of the standard assembly technique, simplicity of implementation, the continuity and the compatibility of the FEM and BEM elements.

The accuracy of the proposed method to solve linear elastic crack problems in fracture mechanics was examined, by calculating the stress intensity factor K_I. This paper used two different techniques implemented in the FEM–BEM program developed. Configurations studied for the comparison are, two symmetrical cracks emanating from a circular hole and a central crack, both in rectangular sheets subjected to tensile loading. It is important to note, that the coupling FEM–BEM using J-integral technique gives very accurate results when compared to the FEM and analytical solutions available in the literature. Furthermore, the J-integral technique is numerically more stable than the displacement extrapolation technique using quarter-point elements. The accuracy of the latter seems to be relatively better when using the FEM–BEM coupling method in comparison with the FE method.

The coupling method presented here can be easily implemented and is a versatile tool for the determination of SIFs in fractured structures of varied shapes not commonly found in handbooks. Furthermore, such high level of accuracy was easily achieved with no more than a few elements along the cracks. It can be seen that the coupling method presented in this paper could be an extremely powerful method for analysing a wide range of problems. The present study will be extended to nonlinear problems.

References

Adey, R.A., Brebbia, C.A., 1983. Basic Computational Techniques for Engineers. Pentech Press, London.

Alvarez-Rubio, S., Benito, J.J., Sanchez-Sesma, F.J., Alarcon, E., 2005. The use of direct boundary element method for gaining insight into complex seismic site response. Comput. Struct. 83, 821–835.

Aour, B., 1997. Couplage FEM-DBEM singulières pour l'analyse des problèmes d'elastostatique bidimensionnels. Thèse de Magister, USTO, Oran.

Aour, B., Rahmani, O., Nait-Abdelaziz, M., 2005. A coupling finite element-boundary element technique for 2-D fracture mechanics problems. 13th French-Polish seminar, Polytech'Lille, France.

Banerjee, P.K., Butterfield, R., 1981. Boundary Element Methods in Engineering Science, second ed. McGraw-Hill, London, UK.
Barsoum, R.S., 1976. On the use of isoparametric finite elements in linear fracture mechanics. Int. J. Numer. Methods Engng. 10, 25–37.
Beer, G., 1986. Implementation of combined boundary element-finite element analysis with application in geomechanics. In: Banerjee, P.K., Watson, J.O. (Eds.), Developments in BEM-4. Applied Science Publischers Ltd., London (Chapter 7).
Bezerra, L.M., Medeiros, J.M.S., Cesari, F.G., Battistela, P., 2001. Simple numerical techniques using boundary element method for the determination of K_I in fracture mechanics. Transactions, 16.
Brebbia, C.A., 1981. Progress in Boundary Element Methods, vol. 1. Plymouth, Pentech Press.
Brebbia, C.A., Dominguez, J., 1992. Boundary Elements: An Introductory Course. CMP and McGraw-Hill, Southampton and New York.
Brebbia, C.A., Georgiou, P., 1979. Combination of boundary and finite elements in Elastostatics. Appl. Math. Modell. 3, 212–220.
Chan, C.L., Chandra, A., 1991. An algorithm for handling corners in the boundary element method: application to conduction-convection equations. Appl. Math. Modell. 15, 244–255.
Chia-Ching, L., Lawton, E.C., Caliendo, J.A., Anderson, L.R., 1996. An iterative finite element-boundary element algorithm. Comput. Struct. 59 (5), 899–909.
Coda, H.B., Venturini, W.S., Komatsu, J.S., Silva, N.A., 1997. BEM/FEM coupling for the continuum media-frame structure interaction. Int. J. BEM Commun. 8, 73–78.
Elleithy, W.M., Al-Gahtani, H.J., El-Gebeilly, M., 2001. Iterative coupling of BE and FE methods in Elastostatics. Engng. Anal. Boundary Elem. 25, 685–695.
Fleming, M., Chu, Y., Moran, B., Belytschko, T., 1997. Enriched element-free Galerkin methods for crack tip fields. Int. J. Numer. Methods Engng. 40, 1484–1504.
Ganguly, S., Layton, J.B., Balakrishna, C., 2000. Symmetric coupling of multi-zone curved Galerkin boundary elements with finite elements in elasticity. Int. J. Numer. Methods Engng. 48, 633–654.
Grannell, J.J., 1988. BEM-FEM coupling for screen infinite domain potential problems. In: Brebbia, C.A. (Ed.), 6th Int. Conf. on BE Technology X, London, vol. 1.
Griffiths, A.A., 1921. Phil. Trans. Roy. Soc. London, Ser. A. 221, 163.
Guven, I., Madenci, E., 2003. Thermoelastic stress field in a piece-wise homogeneous domain under non-uniform temperature using a coupled boundary and finite element method. Int. J. Numer. Methods Engng. 56, 381–403.
Harrop, L.P., 1982. The optimum size of quarter-point crack tip elements. Int. J. Numer. Methods Engng., 1101–1103.
Hellen, T.K., 1975. On the method of virtual crack extension. Int. J. Numer. Methods Engng. 9 (1), 187–208.
Hsiao, G.C., 1988. The coupling of BEM and FEM – a brief review. Boundary Elements X. Computational Mechanics, Southampton, pp. 431–445.
Hunter, P., 2001. FEM/BEM notes. Copyright, Departement of Engineering Science, The University of Auckland, New Zealand.
Li, H-B., Han, G-M., Mang, H.A., Torzchy, Y.P., 1986. A new method for the coupling of finite element and boundary element discretized subdomains of elastic bodies. Comput. Methods Appl. Mech. 54, 161–185.
Owen, D.R.J., Fawkes, A.J., 1983. Engineering Fracture Mechanics. Pineridge Press LTD, Swansea.
Oysu, C., Fenner, R.T., 2006. Coupled FEM–BEM for elastoplastic contact problems using Lagrange multipliers. Appl. Math. Modell. 30, 231–247.
Popov, V., Power, H., 2001. An O(N) Taylor series multipole boundary element method for three-dimensional elasticity problems. Engng. Anal. Bound. Elem. 25, 7–18.
Portela, A., Aliabadi, M.H., 1989. On the accuracy of boundary and finite element techniques for crack problems in fracture mechanics. In: Advances in Boundary Elements. In: Brebbia, C.A., Connor, J.J. (Eds.), Computations and Fundamentals, vol. I. Computational Mechanics Publications, Southampton.
Rice, J.R., 1974. A path-independent integral and the approximate analysis of strain concentration by notches and cracks Trans ASME. J. Appl. Mech. 35, 485–502.
Schnack, E., Turke, K., 1997. Domain decomposition with BEM and FEM. Int. J. Numer. Methods Engng. 40, 2593–2610.
Tada, H., Paris, P.C., Irwin, G.R., 1973. Stress Analysis of Cracks Handbook. Hellertown, USA.
Wearing, J.L., Sheikh, M.A., 1988. A combined finite element boundary element technique for stress analysis. In: Brebbia, C.A. (Ed.), 6th International Conference on Boundary Element Technology X, vol. 1. Computational Mechanics Publications, London.
Woo, C., Wang, Y., Cheung, Y., 1989. The mixed mode problems for the cracks emanating from a circular hole in finite plate. Engng. Fract. Mech. 32, 279–288.
Zienkiewicz, O.C., Kelly, D.W., Bettes, P., 1977. The coupling of the finite element method and boundary solutions procedures. Int. J. Numer. Methods Engng. 11, 355–375.